Journal of Materials Chemistry B

Aqueous Surface Gels as Low Friction Interfaces to Mitigate Implant-Associated Inflammation

Journal:	*Journal of Materials Chemistry B*
Manuscript ID	TB-COM-03-2020-000582.R1
Article Type:	Perspective
Date Submitted by the Author:	04-Apr-2020
Complete List of Authors:	Chau, Allison; University of California Santa Barbara, Materials Rosas, Jonah; University of California Santa Barbara, Biomolecular Science and Engineering Department Degen, George; University of California Santa Barbara, Department of Chemical Engineering Månsson, Lisa; Chalmers University of Technology, Department of Applied Physics Chen, Jonathan; University of California Santa Barbara, Department of Chemical Engineering Valois, Eric; University of California Santa Barbara, Department of Molecular, Cellular, and Developmental Biology Pitenis, Angela; University of California Santa Barbara, Materials

Aqueous Surface Gels as Low Friction Interfaces to Mitigate Implant-Associated Inflammation

Allison L. Chau, [a] Jonah Rosas, [b] George D. Degen, [c] Lisa K. Månsson, [d] Jonathan Chen [c], Eric Valois, [e] and Angela A. Pitenis * [a]

[a] Materials Department
University of California, Santa Barbara
Santa Barbara, CA 93106

[b] Biomolecular Science and Engineering Department
University of California, Santa Barbara
Santa Barbara, CA 93106

[c] Department of Chemical Engineering
University of California, Santa Barbara
Santa Barbara, CA 93106

[d] Department of Physics
Chalmers University of Technology
412 58 Gothenburg, Sweden

[e] Department of Molecular, Cellular, and Developmental Biology
University of California, Santa Barbara
Santa Barbara, CA 93106

***Corresponding Author**

Prof. Angela A. Pitenis
Materials Department
University of California, Santa Barbara
Santa Barbara, CA 93106

email: apitenis@ucsb.edu

Graphical Abstract

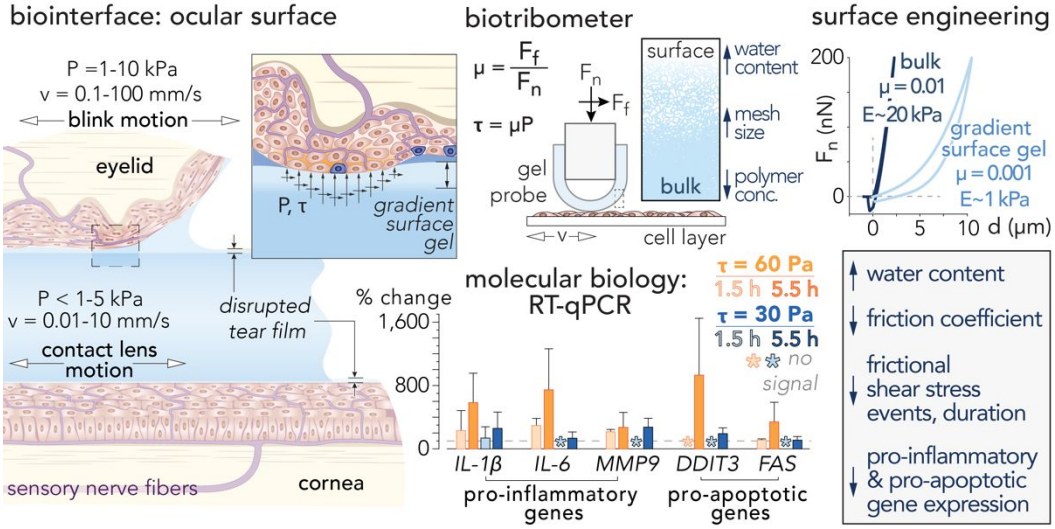

Abstract

Aqueous surface gels are fragile yet resilient biopolymer-based networks capable of sustaining extremely low friction coefficients despite tribologically-challenging environments. These superficial networks are ubiquitous in natural sliding interfaces and protect mechanosensitive cells from excessive contact pressures and frictional shear stresses from cell-fluid, cell-cell, or cell-solid interactions. Understanding these complex lubrication mechanisms may aid in the development of materials-based strategies for increasing biocompatibility in medical devices and implants. Equally as important is characterizing the interplay between soft and passive, yet mobile implant materials and cellular reactions in response to direct contact and frictional shear stresses. Physically interrogating living biological systems without rupturing them in the process is nontrivial. To this end, custom biotribometers have been designed to precisely modulate contact pressures against living human telomerase-immortalized corneal epithelial (hTCEpi) cell layers using soft polyacrylamide membrane probes. Reverse-transcription quantitative polymerase chain-reaction (RT-qPCR) indicated that increased duration, and to a much greater extent, the magnitude of frictional shear stress, leads to increased production of pro-inflammatory (*IL-1β, IL-6, MMP9*) and pro-apoptotic (*DDIT3, FAS*) genes, which in clinical studies are linked to pathological pain. The hierarchical structure often found in biological systems has also been investigated through the fabrication of high-water content (polyacrylamide) hydrogels through free-radical polymerization inhibition. Nanoindentation experiments and friction coefficient measurements indicate that these "gradient surface gels" reduce contact pressures and frictional shear stresses at the surface of the material while still maintaining stiffness within the bulk of the material. Reducing frictional shear stresses through informed materials and surface design may concomitantly increase lubricity and quiet the immune response, and thus provide bio-inspired routes to improve patient outcomes and quality of life.

Introduction

Lubrication across tissue interfaces, within our joints, and across synthetic/biological interfaces is essential to maintain health, mobility, homeostasis, and provide pain-free (comfort) interfacial slip during daily activities[1]. Classical lubrication theory (Figure 1a,b) is frequently invoked to describe the transient and dynamic interfacial and energy-dissipative phenomena between two impermeable surfaces sliding in relative motion [2]. However, no single unifying theory yet exists to describe the complex lubrication mechanisms between highly deformable, permeable, and aqueous gel surfaces (Figure 1c). Over the past decade, engineers and scientists have looked to the Stribeck curve (Figure 1d) as a foundation upon which to characterize lubrication behavior of biological interfaces both in homeostasis and far from equilibrium. In the event of injury, illness, or implants, the body's natural lubrication mechanisms may become compromised, which could initiate a positive feedback loop of increasingly inflammatory conditions [3,4]. Medical implants may impair the body's natural lubrication strategies by increasing local contact pressures and shear stresses against endogenous cells, cell layers, and tissues beyond physiological norms[5,6]. Increased contact pressures and/or decreased sliding velocities may force natural sliding interfaces away from fluid film lubrication and towards boundary lubrication[2] thus increasing friction coefficients and increasing the risk of cell damage. Although the contributions of implant-associated friction to the onset and progression of disease have remained poorly understood, links between friction and inflammation reverberate throughout the literature, from contact lenses[7–12] to breast implants[13–16] and from stents[17–19] to catheters[20–22].

Many cells, including epithelial and endothelial cells, have the ability to respond shear stress, and on some interfaces form a primitive sensor network through the expression of soluble and surface proteins, and their interactions with receptor proteins. The process by which cells physically sense and biochemically respond to the local environment is known as mechanotransduction [23]. However, the precise mechanisms by which transmembrane proteins transmit physical signals to the nucleus and alter the phenotype remain unclear. Multiple biological components are thought to activate and participate in mechanotransduction pathways [24] (Figure 2).

The glycocalyx, a dynamic and very lightly crosslinked biopolymer-based hydrogel [25] composed of heavily glycosylated transmembrane mucins on the cell surface, may mediate mechanotransduction signaling in response to compressive stress [26,27], fluid shear stress [28–31] and frictional shear stress [27,32,33]. Stretch-activated ion channels in the apical cell membrane open in response to strain and permit influx of potassium [34], calcium [35], sodium [36], and other ions [37]. Concentrations of cell-signaling molecules may change during cell deformations (e.g., compression, mechanical confinement) [38,39]. Cell-cell and cell-matrix adhesion complexes enable cells and tissues to probe local environments [40]. Extracellular matrix proteins (e.g., fibronectin, collagen) can undergo force-induced protein unfolding and initiate mechanotransduction signaling outside the cell [41]. Intracellular strain can provoke conformational changes in cytoskeletal filaments and crosslinking proteins, consequently altering binding affinities to specific molecules and activating mechanotransduction signaling pathways [42,43]. The nuclear envelope is mechanically linked to the extracellular matrix (ECM) by force-transmitting cytoskeletal

filaments. Nuclear mechanosensing is achieved through several pathways, including stress-induced protein conformational changes, transcriptional regulator translocation, chromosome conformation and organization, and membrane deformation [44]. Recent studies suggest that even chromatin itself is mechanosensitive [45]. For nearly all cells, mechanical stimulations induce adaptive changes in cell function, from short-term responses (e.g., changes in intracellular tension, adhesion, migration) to long-term effects (e.g., protein secretion, structural reorganization, proliferation, viability) [46]. These responses are often mediated through a plurality of signaling pathways that may overlap and even cross-talk [47], complicating definitive identification of the primary mechanosensor(s) [24].

The mechanics and dynamics of mechanotransduction

Cells have developed complex features to mediate function and gene expression in response to physical phenomena such as flow and contact pressure. Shear mechanics play a critical role in shaping cellular fate and function, prompting the evolution of mechanosensitive responses that have remained highly conserved across broad evolutionary timescales. Fluid and frictional shear stresses are two key avenues by which cells understand their environment and interpret the mechanics and the mechanical forces associated with their local environment, which is distinct from the environmental context associated with local proteins, growth factors, and signaling milieu. The inability of cells to appropriately interpret these forces have been implicated in the onset of various morphological defects and the progression of disease[24].

Both fluid shear stress and frictional shear stress are present in the body but have different drivers and components of stress. Fluid shear stress results from velocity gradients within a liquid due to viscosity. For a Newtonian fluid of dynamic viscosity μ, the shear stress τ at a boundary can be calculated as

$$\tau = \mu(\mathrm{d}u/\mathrm{d}y)$$

where u is the velocity parallel to the boundary and y is the coordinate normal to the boundary. The molecular origins of viscosity, and thus fluid shear stress, are momentum exchange between fluid molecules due to intermolecular interactions. If the properties of the fluid are known, the fluid shear stress can be calculated from measurements of fluid velocity and relatively few assumptions (e.g., incompressible fluid, no-slip boundary).

At the solid-fluid boundary, complex flow behavior has a rich history but more recently, fluid dynamics has been applied to understand the manners in which biological systems use interstitial flow for organism-level remodeling. *In vitro* mechanobiology studies of endothelial[48,49] and epithelial[50,51] cell layers indicate that cells are sensitive to less than a single Pa of fluid shear stress and furthermore respond depending on the orientation, duration, or magnitude of the fluid shear stress. Ng *et al.* have probed the role of low interstitial flow rates in triggering endothelial cell morphogenesis, highlighting vastly unique 3D structures in lymphatic and blood endothelial cells based on differences in the cells' biophysical environment [52]. Because interstitial flow plays key roles in tissue and organ development, disease onset and progression, and ECM remodeling, a comprehensive inquiry of mechanotransduction is necessary to appreciate how cells decode

information about their environment, and how mutations in these information highways result in morphological defects, disease, and cell death [53–55].

Cells are regularly exposed to cell-cell and cell-solid sliding interfaces. It is at these interfaces that cells experience frictional shear stresses, which result from molecular interactions occurring between solids in contact or close proximity at an interface. Soft and hard implants (e.g., stents, ports, drains, and catheters) impart additional tribological challenges upon endogenous biological tissues that are physically distinct from fluid shear stresses, which lack a normal component of stress.

In contrast with fluid shear stresses, frictional shear stresses are difficult to model, as they can result from competing bonds of different energies and length- and timescales [56]. The first observations of friction were recorded by Leonardo da Vinci between 1480 and 1518, later described by G. Amontons in 1699, and again confirmed by C. Coulomb in 1785 [57,58]. The simple laws of friction, derived from Amontons' publications, state that the friction force F_f is proportional to the applied load F_n and independent of the contact area, represented by the equation

$$F_f = \mu F_n$$

where the proportionality constant μ is the coefficient of friction. Here, the simple proportionality results from compression of asperities and an increase in the real area of contact with increasing load. Dividing by the contact area, A, recasts the equation in terms of frictional shear stress, τ, and contact pressure, P

$$\tau = \mu P$$

This simple relationship stresses the importance of both low friction coefficients and low contact pressures in achieving lubricity. As an illustrative example, scalpels may exhibit low surface roughness and low friction coefficients, but also high contact pressures which can easily rupture cell membranes.

The earliest studies of frictional shear stress on cells found that frictional stress resulted in the thickening of the stratum corneum and an increase in proliferation [59]. Studies have also implicated frictional shear stress in the onset of corneal epithelial cell inflammation, highlighting the disparate manner in which various cell-types are able to adapt and overcome frictional shear stresses [9,33]. In 1990, Talja *et al.* [60] investigated the role of catheter surface materials in a clinical study, and observed increased inflammatory reactions in urethral epithelial cells subjected to increased friction. Recent *in vitro* studies have observed friction-induced inflammation and apoptosis in corneal epithelial cell monolayers at frictional shear stresses on the order of 40-60 Pa [27]. Systematically interrogating how cells respond to magnitude, orientation, and duration of frictional shear stress may better inform the design of soft medical devices deployed over short timescales (e.g., contact lenses, endotracheal tubes, catheters) and those used over much longer timescales (e.g., intraocular lenses, shunts, stents, intrauterine devices).

Soft and Fragile Interfaces in Biology

Soft biological interfaces largely comprise fragile yet protective three-dimensional networks of hydrophilic biopolymers, or mucin gels. These gel-spanning networks act as

mechanical fuses at high shear rates and dissipate energy at a safe distance from the mechanosensitive epithelium below. For healthy individuals, mucin gel layer thicknesses range from ~5 μm in the ocular tear film [61], 10-20 μm in airways[62], and >500 μm in the intestines [63]. The measured mesh size [64], or average spacing between neighboring polymer chains in mucin gels, is approximately 100-500 nm [62]. A more straightforward measurement (yet not without its challenges) is water content, which is typically 90-98% for most mucosal surfaces [65]. This method facilitates tribological comparisons across very different systems, for instance: mucus (biopolymer hydrogels) and synthetic hydrogels (Figure 3).

Hydrogels have been widely used across mechanobiology [66–68] rheology[69], and tribology [70,71] studies due to their high water content, transparency, tunable mechanical properties, and ease of polymerization. Recent studies have suggested that a single parameter, the polymer mesh size, ξ, drives not only the mechanical and transport properties [64], but also the lubrication properties of hydrogels [72]. Increasing the mesh size increases the water content, decreases the elastic modulus, and decreases the friction coefficient.

Tools for biotribology

Hertzian contact mechanics dictates that the composite elastic modulus, E^*, sets the contact pressure, P ($P \sim E^{*2/3}$). Thus, even qualitatively "soft" hydrogels may impart signigicant contact pressures in excess of 10's of kPas on living cell layers (the elastic modulus of which are typically 10's of kPas [73]), effectively rupturing cell membranes upon first contact. Achieving physiologically-relevant contact pressures for biotribological studies requires completely different probe geometries. Within the limit of low forces, spherical shell membrane probes[74] leverage membrane mechanics to set constant contact pressures (typically around 1 kPa) regardless of fluctuations in applied normal load during tribological testing on living cell layers (Figure 4).

Contact pressures may be calculated from controlled indentations on an inverted widefield fluorescence microscope. Hydrogel membrane probes may be molded or 3D printed [75–78] and the geometry is compatible with several types of materials, including polyacrylamide (PAAm), polyethylene glycol (PEG), polyhydroxyethylmethacrylate (PHEMA), poly(N-isopropylacrylamide) (PNIPAm), and even non-aqueous materials like polydimethylsiloxanesilicone (PDMS) and silicones. Spherical shell membrane probes may also be manufactured from actual soft implant materials (e.g., contact lens strips). In this work, hydrogel membrane probes were molded from PAAm. Membrane probes may be fabricated with a range of thicknesses, t, to target desired contact pressures, P, against extracellular matrix components, cells, cell layers, and tissues. Friction coefficients, μ, measured during sliding experiments, are multiplied by the contact pressure to calculate frictional shear stress. While the elastic modulus ($P \sim E$) and the friction coefficient ($\tau \sim \mu$) may also affect the contact pressure and frictional shear stress, respectively, the dependence on probe thickness is much greater ($P, \tau \sim t^2$).

Molecular biotribology: A window into cellular mechanotransduction

Biotribometers are instruments designed to measure normal and friction forces of biological materials (cells, cell layers, and tissues) with micronewton precision and have been described previously[79] (Figure 5a). These custom-built instruments are designed with an integrated incubation chamber to maintain cell culture conditions during extended duration sliding experiments (1 mm/s sliding speeds, upwards of 10,000 reciprocating cycles[32]). Soft hydrogel membrane probes have been frequently used to contact and slide against living cell layers. Corneal epithelial cells have frequently been selected for biotribology studies because cornea-eyelid and the cornea-contact lens sliding interfaces may be approximated as sphere-on-flat reciprocating contacts. Human telomerase-immortalized corneal epithelial (hTCEpi) cell monolayers[80] are excellent candidate cells for biotribology studies due to their similarities to their natural analogs in growth, proliferation, differentiation, and secretion of transmembrane mucins MUC1, MUC4, and MUC16. These hTCEpi cells are cultured and plated according to previous methods[33] within a custom differential culture dish. This design separates two identical cell populations to compare changes in gene expression in response to frictional shear stresses with a reference using molecular biology techniques, including reverse-transcriptase quantitative polymerase chain-reaction (RT-qPCR) (Figure 5b). Following targeted frictional shear stresses of τ = 30 Pa, gene expression between the testing and reference cell populations are largely unchanged from baseline control measurements (within 100% change) compared to a housekeeping gene β-actin (Figure 5c). However, increased frictional shear stresses τ = 60 Pa induces significant increases in both pro-inflammatory (*IL-1β, IL-6, MMP9*) and pro-apoptotic (*DDIT3, FAS*) genes linked to pathological pain[81,82] (Figure 5d). The findings herein suggest that pro-inflammatory and pro-apoptotic gene expression also increases with increased sliding duration (from 1.5 h to 5.5 h) yet it is clear that the magnitude of frictional shear stress is the predominant driver. Despite the limitations of these experiments (tests were performed in monolayer, homogenous monoculture, and against fibronectin-coated glass coverslips), these *in vitro* results suggest that *in vivo* immunomodulation may be tractable through rational surface design of implant materials.

Recent unpublished studies have also utilized enzyme-linked immunosorbent assays (ELISA) to sample growth media prior to, during, and following tribological experiments. Other studies have used fluorescence microscopy to identify the onset and progression of apoptosis in cell monolayers in situ via live-cell staining, finding no increase in cell death for pure compression (τ = 0 Pa) and a clear threshold of τ = 40-60 Pa for the initiation of apoptosis [27]. Future studies may also utilize flow cytometry, Western blots, or additional molecular biology techniques to examine gene expression changes arising purely from frictional shear stresses.

Designing for Biocompatibility

It is well understood that there is no such thing as a biocompatible material [83]. Instead, designing for biocompatibility involves the informed design of biocompatible systems. In addition to the guidance enclosed in International Standard ISO 10993-1, "Biological evaluation of medical devices - Part 1: Evaluation and testing within a risk management process" the results of recent

studies[27,33] warrant further consideration of cellular responses to direct contact and frictional shear stresses. It may be illuminating to revisit all FDA-approved materials for soft implants and evaluate them based on their tribological behavior when sliding against cell layers and cell multilayers in co-culture (e.g., with fibroblasts, known to mediate inflammatory responses in vivo [84]).

In the interim, reducing deleterious impacts of biomaterials -- both chemically and physically -- interacting with endogenous cells, cell layers, tissues, and organs, is of paramount importance. A bio-inspired approach involves borrowing design rules from nature and applying them to new materials and interfaces. Recently, reducing contact pressures and frictional shear stresses at the surface while maintaining stiffness within the bulk of the material has recently been achieved by means of near-substrate gel polymerization [70,85–88] and by delamination of gel surface layers[89]. Free-radical polymerization inhibition has recently been used to fabricate gradient surface gels with very high-water content at the superficial layer (Figure 6a). Previous studies showed that the sliding interface of two self-mated or "Gemini" hydrogels, albeit one with a gradient gel structure, is considered "superlubricious" with friction coefficients as low as μ = 0.001. In comparison, a bulk Gemini interface of the same initial polymer concentration (7.5 wt.% PAAm) but without the hierarchical gel-spanning network has a friction coefficient about an order of magnitude above, μ = 0.01 (Figure 6b). Nanoindentations of the superficial and bulk layers of the hydrogel with a spherical silica probe (5 μm radius) indicate that the gradient surface gel may be about 20 times softer than the bulk (Figure 6c, d). This synthetic, "cell-inspired" material was structurally complex and compositionally-graded, and exhibited the stiffness of a typical mammalian cell in the bulk (~20 kPa), yet the softness of a fully swollen mucin gel network at the surface (<1 kPa).

Recent characterization efforts through atomic force microscopy have identified that the "gradient surface gel" at the superficial region displays marked contact hysteresis during nanoindentation, possibly due to poroelastic or viscoelastic responses during loading, which agrees with previous efforts by other groups[90,91] yet the complex interplay between hydrophilic polymers of the hydrogel network and water (the solvent and the major phase of the gradient surface gel network) complicates a classical treatment of the contact mechanics, and necessitates further study.

Concluding remarks

Aqueous biological interfaces are extremely soft and slippery. Nature designs biocompatible material systems with extremely high-water content and thus high mesh size at the surface to promote lubricity where it is needed, and lower water content and lower mesh size at the subsurface to maintain mechanical and barrier properties. Aqueous gel surfaces in biology are often soft and compliant, which further diminish shear stresses and thus friction coefficients. Low shear stress is typically accompanied by a quiescent immune response, and may decrease rates of reported discomfort and/or pain in case an implant must be introduced to improve form or function.

Conflicts of interest

There are no conflicts of interest to declare.

Acknowledgements

The research reported here made use of shared facilities of the National Science Foundation (NSF) Materials Research Science and Engineering Center at UC Santa Barbara, DMR-1720256. The UCSB MRSEC is a member of the Materials Research Facilities Network (www.mrfn.org). A.L.C., L.K.M., and E.V. were supported by the UCSB MRSEC Program of the National Science Foundation under Award No. DMR-1121053. J.R. was supported by the Bill and Melinda Gates Foundation. G.D.D. was supported by the National Science Foundation Graduate Research Fellowship Program under Grant No. 1650114. The authors acknowledge support from the California NanoSystems Institute (CNSI) Challenge Grant program.

References

1 D. Dowson, *Proc. Inst. Mech. Eng. Part J J. Eng. Tribol.*, 2009, **223**, 261–273.
2 B. J. Hamrock, S. R. Schmid and B. O. Jacobson, *Fundamentals of fluid film lubrication*, Marcel Dekker, Inc., New York, 2nd Ed., 2004.
3 C. Baudouin, M. Rolando, J. M. Benitez Del Castillo, E. M. Messmer, F. C. Figueiredo, M. Irkec, G. Van Setten and M. Labetoulle, *Prog. Retin. Eye Res.*, 2019, **71**, 68–87.
4 J. M. Anderson, A. Rodriguez and D. T. Chang, *Semin. Immunol.*, 2008, **20**, 86–100.
5 A. C. Dunn, J. A. Tichy, J. M. Urueña and W. G. Sawyer, *Tribol. Int.*, 2013, **63**, 45–50.
6 G. Rocatello, N. El Faquir, G. De Santis, F. Iannaccone, J. Bosmans, O. De Backer, L. Sondergaard, P. Segers, M. De Beule, P. de Jaegere and P. Mortier, *Circ. Cardiovasc. Interv.*, , DOI:10.1161/CIRCINTERVENTIONS.117.005344.
7 N. Efron, *Clin. Exp. Optom.*, 1985, **68**, 167–172.
8 N. Efron, *Br. J. Ophthalmol.*, 2012, **96**, 1447–1448.
9 Y. Alzahrani, L. Colorado, N. Pritchard and N. Efron, *Optom. Vis. Sci.*, 2016, **93**, 917–924.
10 N. Efron, *Clin. Exp. Optom.*, 2017, **100**, 3–19.
11 N. Efron, *Clin. Exp. Optom.*, 2018, **101**, 1–3.
12 A. López-de la Rosa, I. Fernández, C. García-Vázquez, C. Arroyo-del Arroyo, M. J. González-García and A. Enríquez-de-Salamanca, *Ocul. Immunol. Inflamm.*, 2019, 1–20.
13 S. Mauro, F. Eugenio and B. Roberto, *Aesthetic Plast. Surg.*, 2005, **29**, 10–12.
14 W. Peters and V. Fornasier, *Can. J. Plast. Surg.*, 2007, **15**, 19–28.
15 M. Mazzocchi, L. A. Dessy, F. Corrias and N. Scuderi, *Aesthetic Plast. Surg.*, 2012, **36**, 97–104.
16 A. M. Munhoz, M. W. Clemens and M. Y. Nahabedian, *Plast. Reconstr. Surg. - Glob. Open*, 2019, **7**, e2466.
17 L. Cormio, M. Talja, A. Koivusalo, H. Makisalo, H. Wolff and M. Ruutu, *J. Urol.*, 1995, **153**, 494–496.
18 A. Fortier, V. Gullapalli and R. A. Mirshams, *IJC Hear. Vessel.*, 2014, **4**, 12–18.
19 N. Laube, C. Desai, F. Bernsmann and C. Fisang, *Springerplus*, 2015, **4**, 247.
20 D. Graiver, R. L. Durall and T. Okada, *Biomaterials*, 1993, **14**, 465–469.
21 J. Stensballe, D. Looms, P. N. Nielsen and M. Tvede, *Eur. Urol.*, 2005, **48**, 978–983.
22 M. J. Andersen and A. L. Flores-Mireles, *Coatings*, 2019, **10**, 23.
23 E. K. Paluch, C. M. Nelson, N. Biais, B. Fabry, J. Moeller, B. L. Pruitt, C. Wollnik, G. Kudryasheva, F. Rehfeldt and W. Federle, *BMC Biol.*, 2015, **13**, 47.
24 D. E. Jaalouk and J. Lammerding, *Nat. Rev. Mol. Cell Biol.*, 2009, **10**, 63–73.
25 O. Lieleg, I. Vladescu and K. Ribbeck, *Biophys. J.*, 2010, **98**, 1782–1789.
26 J.-A. Park and D. J. Tschumperlin, *Am. J. Respir. Cell Mol. Biol.*, 2009, **41**, 459–466.
27 S. M. Hart, G. D. Degen, J. M. Urueña, P. P. Levings, W. G. Sawyer and A. A. Pitenis, *Tribol. Lett.*, 2019, **67**, 82.
28 S. Weinbaum, X. Zhang, Y. Han, H. Vink and S. C. Cowin, *Proc. Natl. Acad. Sci.*, 2003, **100**, 7988–7995.
29 J. M. Tarbell and M. Y. Pahakis, *J. Intern. Med.*, 2006, **259**, 339–350.
30 C. C. DuFort, M. J. Paszek and V. M. Weaver, *Nat. Rev. Mol. Cell Biol.*, 2011, **12**, 308–319.
31 M. A. Dragovich, D. Chester, B. M. Fu, C. Wu, Y. Xu, M. S. Goligorsky and X. F. Zhang, *Am. J. Physiol. Physiol.*, 2016, **311**, C846–C853.
32 A. A. Pitenis, J. M. Urueña, T. T. Hormel, T. Bhattacharjee, S. R. Niemi, S. L. Marshall, S.

M. Hart, K. D. Schulze, T. E. Angelini and W. G. Sawyer, *Biotribology*, 2017, **11**, 77–83.
33 A. A. Pitenis, J. M. Urueña, S. M. Hart, C. S. O'Bryan, S. L. Marshall, P. P. Levings, T. E. Angelini and W. G. Sawyer, *Tribol. Lett.*, 2018, **66**, 81.
34 L. Lu, *Prog. Retin. Eye Res.*, 2006, **25**, 515–538.
35 A. W. Orr, B. P. Helmke, B. R. Blackman and M. A. Schwartz, *Dev. Cell*, 2006, **10**, 11–20.
36 S.-I. Watanabe, M. Tanizaki and A. Kaneko, *Exp. Eye Res.*, 1997, **64**, 1027–1035.
37 S. S. Ranade, R. Syeda and A. Patapoutian, *Neuron*, 2015, **87**, 1162–1179.
38 A. K. T. Wann, N. Zuo, C. J. Haycraft, C. G. Jensen, C. A. Poole, S. R. McGlashan and M. M. Knight, *FASEB J.*, 2012, **26**, 1663–1671.
39 H. Lee, L. Gu, D. J. Mooney, M. E. Levenston and O. Chaudhuri, *Nat. Mater.*, 2017, **16**, 1243–1251.
40 L. Ramage, G. Nuki and D. M. Salter, *Scand. J. Med. Sci. Sports*, 2009, **19**, 457–469.
41 J. D. Humphrey, E. R. Dufresne and M. A. Schwartz, *Nat. Rev. Mol. Cell Biol.*, 2014, **15**, 802–812.
42 F. Martino, A. R. Perestrelo, V. Vinarský, S. Pagliari and G. Forte, *Front. Physiol.*, , DOI:10.3389/fphys.2018.00824.
43 T. Luo, K. Mohan, P. A. Iglesias and D. N. Robinson, *Nat. Mater.*, 2013, **12**, 1064–1071.
44 P. Isermann and J. Lammerding, *Curr. Biol.*, 2013, **23**, R1113–R1121.
45 S. Cho, J. Irianto and D. E. Discher, *J. Cell Biol.*, 2017, **216**, 305–315.
46 M. Bai, L. Cai, X. Li, L. Ye and J. Xie, *J. Biomed. Mater. Res. Part B Appl. Biomater.*, 2020, jbm.b.34575.
47 G. Vert and J. Chory, *Dev. Cell*, 2011, **21**, 985–991.
48 C. F. Dewey, S. R. Bussolari, M. A. Gimbrone and P. F. Davies, *J. Biomech. Eng.*, 1981, **103**, 177–185.
49 R. Sinha, S. Le Gac, N. Verdonschot, A. van den Berg, B. Koopman and J. Rouwkema, *Sci. Rep.*, 2016, **6**, 29510.
50 S. Molladavoodi, M. Robichaud, D. Wulff and M. Gorbet, *PLoS One*, 2017, **12**, e0178981.
51 E. W. Flitney, E. R. Kuczmarski, S. A. Adam and R. D. Goldman, *FASEB J.*, 2009, **23**, 2110–2119.
52 C. P. Ng, C.-L. E. Helm and M. A. Swartz, *Microvasc. Res.*, 2004, **68**, 258–264.
53 S. Hammerschmidt, H. Kuhn, C. Gessner, H.-J. Seyfarth and H. Wirtz, *Am. J. Respir. Cell Mol. Biol.*, 2007, **37**, 699–705.
54 J. A. Pedersen, S. Lichter and M. A. Swartz, *J. Biomech.*, 2010, **43**, 900–905.
55 C. R. White and J. A. Frangos, *Philos. Trans. R. Soc. B Biol. Sci.*, 2007, **362**, 1459–1467.
56 J. Israelachvili, *Intermolecular and Surface Forces*, Academic Press, 3rd Editio., 2011.
57 D. Dowson, *History of Tribology*, Longman Group Ltd., London, 1979.
58 A. A. Pitenis, D. Dowson and W. Gregory Sawyer, *Tribol. Lett.*, 2014, **56**, 509–515.
59 I. C. Mackenzie, in *Stratum Corneum*, Springer Berlin Heidelberg, Berlin, Heidelberg, 1983, pp. 153–160.
60 M. Talja, A. Korpela and K. Järvi, *Br. J. Urol.*, 1990, **66**, 652–657.
61 M. D. P. Willcox, P. Argüeso, G. A. Georgiev, J. M. Holopainen, G. W. Laurie, T. J. Millar, E. B. Papas, J. P. Rolland, T. A. Schmidt, U. Stahl, T. Suarez, L. N. Subbaraman, O. Ö. Uçakhan and L. Jones, *Ocul. Surf.*, 2017, **15**, 366–403.
62 G. A. Duncan, J. Jung, J. Hanes and J. S. Suk, *Mol. Ther.*, 2016, **24**, 2043–2053.
63 M. Ruponen and A. Urtti, *Eur. J. Pharm. Biopharm.*, 2015, **96**, 442–446.
64 P.-G. De Gennes, *Scaling Concepts in Polymer Physics*, Cornell University Press, 1979.

65 S. K. Lai, Y.-Y. Wang, D. Wirtz and J. Hanes, *Adv. Drug Deliv. Rev.*, 2009, **61**, 86–100.
66 D. E. Discher, *Science (80-.).*, 2005, **310**, 1139–1143.
67 A. J. Engler, S. Sen, H. L. Sweeney and D. E. Discher, *Cell*, 2006, **126**, 677–689.
68 A. K. Denisin and B. L. Pruitt, *ACS Appl. Mater. Interfaces*, 2016, **8**, 21893–21902.
69 C. A. Grattoni, H. H. Al-Sharji, C. Yang, A. H. Muggeridge and R. W. Zimmerman, *J. Colloid Interface Sci.*, 2001, **240**, 601–607.
70 J. P. Gong, *Soft Matter*, 2006, **2**, 544–552.
71 Y. Gombert, R. Simič, F. Roncoroni, M. Dübner, T. Geue and N. D. Spencer, *Adv. Mater. Interfaces*, 2019, **6**, 1901320.
72 J. M. Urueña, A. A. Pitenis, R. M. Nixon, K. D. Schulze, T. E. Angelini and W. Gregory Sawyer, *Biotribology*, 2015, **1–2**, 24–29.
73 K. D. Schulze, S. M. Hart, S. L. Marshall, C. S. O'Bryan, J. M. Urueña, A. A. Pitenis, W. G. Sawyer and T. E. Angelini, *Biotribology*, 2017, **11**, 3–7.
74 S. L. Marshall, K. D. Schulze, S. M. Hart, J. M. Urueña, E. O. McGhee, A. I. Bennett, A. A. Pitenis, C. S. O'Bryan, T. E. Angelini and W. G. Sawyer, *Biotribology*, 2017, **11**, 69–72.
75 T. Bhattacharjee, S. M. Zehnder, K. G. Rowe, S. Jain, R. M. Nixon, W. G. Sawyer and T. E. Angelini, *Sci. Adv.*, 2015, **1**, e1500655.
76 T. Bhattacharjee, C. J. Gil, S. L. Marshall, J. M. Urueña, C. S. O'Bryan, M. Carstens, B. Keselowsky, G. D. Palmer, S. Ghivizzani, C. P. Gibbs, W. G. Sawyer and T. E. Angelini, *ACS Biomater. Sci. Eng.*, 2016, **2**, 1787–1795.
77 C. S. O'Bryan, T. Bhattacharjee, S. Hart, C. P. Kabb, K. D. Schulze, I. Chilakala, B. S. Sumerlin, W. G. Sawyer and T. E. Angelini, *Sci. Adv.*, 2017, **3**, e1602800.
78 C. S. O'Bryan, T. Bhattacharjee, S. R. Niemi, S. Balachandar, N. Baldwin, S. T. Ellison, C. R. Taylor, W. G. Sawyer and T. E. Angelini, *MRS Bull.*, 2017, **42**, 571–577.
79 J. M. Urueña, S. M. Hart, D. L. Hood, E. O. McGhee, S. R. Niemi, K. D. Schulze, P. P. Levings, W. G. Sawyer and A. A. Pitenis, *Tribol. Lett.*, 2018, **66**, 141.
80 D. M. Robertson, L. Li, S. Fisher, V. P. Pearce, J. W. Shay, W. E. Wright, H. D. Cavanagh and J. V. Jester, *Investig. Opthalmology Vis. Sci.*, 2005, **46**, 470.
81 C. M. B. de Oliveira, R. K. Sakata, A. M. Issy, L. R. Gerola and R. Salomão, *Brazilian J. Anesthesiol.*, 2011, **61**, 255–265.
82 J.-M. Zhang and J. An, *Int. Anesthesiol. Clin.*, 2007, **45**, 27–37.
83 D. F. Williams, *Biomaterials*, 2014, **35**, 10009–10014.
84 S. Van Linthout, K. Miteva and C. Tschope, *Cardiovasc. Res.*, 2014, **102**, 258–269.
85 X. Zhang, J. Xu, K. Okawa, Y. Katsuyama, J. Gong, Y. Osada and K. Chen, *J. Phys. Chem. B*, 1999, **103**, 2888–2891.
86 T. Narita, A. Knaebel, J.-P. Munch, S. J. Candau, J. P. Gong and Y. Osada, *Macromolecules*, 2001, **34**, 5725–5726.
87 A. Kii, J. Xu, J. P. Gong, Y. Osada and X. Zhang, *J. Phys. Chem. B*, 2001, **105**, 4565–4571.
88 M. Peng, J. Ping Gong and Y. Osada, *Chem. Rec.*, 2003, **3**, 40–50.
89 K. Zhang, R. Simic, W. Yan and N. D. Spencer, *ACS Appl. Mater. Interfaces*, 2019, **11**, 25427–25435.
90 E. R. Reale and A. C. Dunn, *Soft Matter*, 2017, **13**, 428–435.
91 T. Shoaib and R. M. Espinosa-Marzal, *Tribol. Lett.*, 2018, **66**, 96.
92 J. P. Gong, T. Kurokawa, T. Narita, G. Kagata, Y. Osada, G. Nishimura and M. Kinjo, *J. Am. Chem. Soc.*, 2001, **123**, 5582–5583.

93 S. Yashima, S. Hirayama, T. Kurokawa, T. Salez, H. Takefuji, W. Hong and J. P. Gong, *Soft Matter*, 2019, **15**, 1953–1959.
94 T. Shoaib, J. Heintz, J. A. Lopez-Berganza, R. Muro-Barrios, S. A. Egner and R. M. Espinosa-Marzal, *Langmuir*, 2018, **34**, 756–765.
95 T. Shoaib and R. M. Espinosa-Marzal, *ACS Appl. Mater. Interfaces*, 2019, **11**, 42722–42733.
96 Y. A. Meier, K. Zhang, N. D. Spencer and R. Simic, *Langmuir*, 2019, **35**, 15805–15812.
97 J. Mandal, R. Simic and N. D. Spencer, *Adv. Mater. Interfaces*, 2019, **6**, 1970094.
98 J. Mandal, R. Simic and N. D. Spencer, *Adv. Mater. Interfaces*, 2019, **6**, 1900321.
99 A. A. Pitenis, J. M. Urueña, K. D. Schulze, R. M. Nixon, A. C. Dunn, B. A. Krick, W. G. Sawyer and T. E. Angelini, *Soft Matter*, 2014, **10**, 8955–8962.
100 S. P. Timoshenko and S. Woinowsky-Krieger, *Theory of Plates and Shells*, McGraw-Hill Book Company, New York, 2nd Editio., 1959.
101 R. J. Roark, *Formulas for Stress and Strain*, McGraw-Hill Book Company, New York, 4th Editio., 1965.
102 A. A. Pitenis, J. Manuel Urueña, A. C. Cooper, T. E. Angelini and W. Gregory Sawyer, *J. Tribol.*, , DOI:10.1115/1.4032890.

Figures and Figure Captions

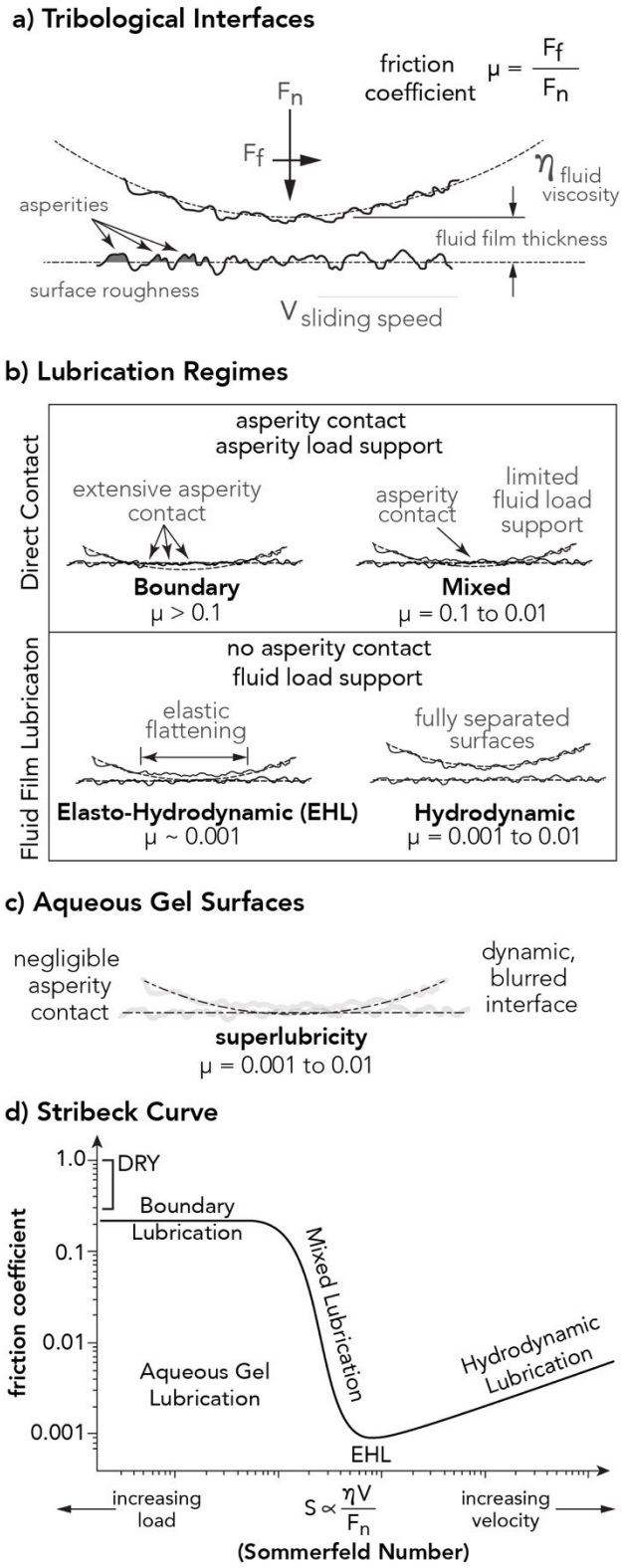

Fig. 1 a) Illustration of a canonical lubricated interface between two rough surfaces in sliding contact subjected to friction F_f and normal F_n forces. The ratio of these forces is the friction coefficient. In the event of insufficient fluid film lubrication, high points, or asperities, on opposing rough surfaces may collide and generate wear debris. b) Schematic of four classical lubrication regimes defined either in

terms of the extent of asperity contact or fluid load support and accompanied by typical ranges of friction coefficients. c) In contrast, aqueous gel surfaces can exhibit "hydrodynamic-like" friction coefficients despite dynamic, blurred interfaces over large contact areas. d) Aqueous gel lubrication is still uncharted on the Stribeck curve, although several groups have put forth tremendous efforts in this area [70,71,91–98]. Adapted from Ref. [99] with permission from the Royal Society of Chemistry.

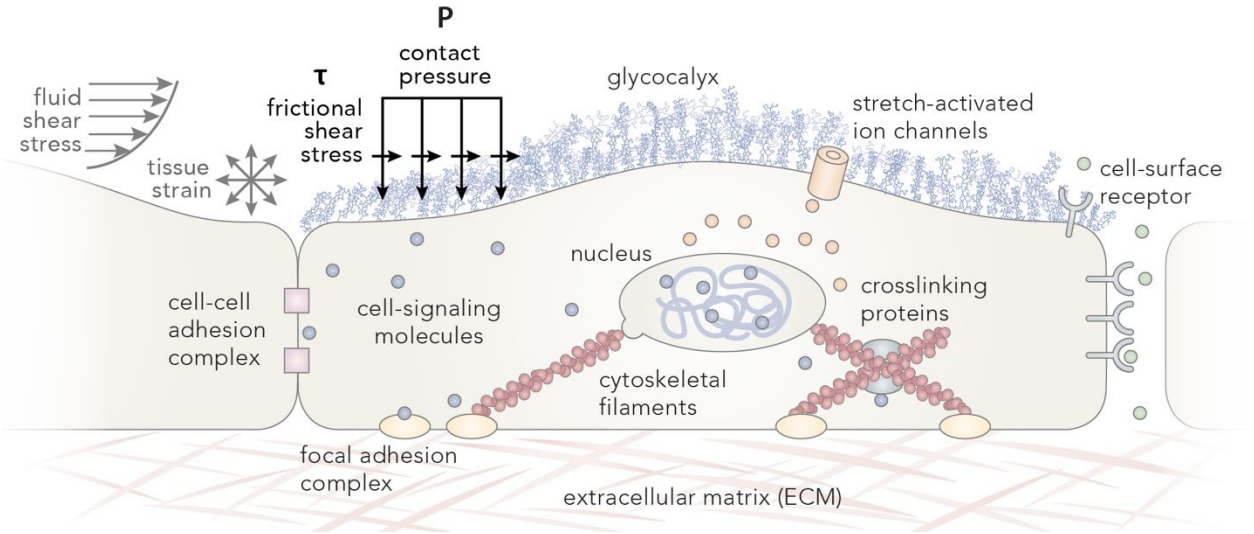

Fig. 2 Cells may sense and respond to mechanical stimuli via multiple mechanosensitive biological components, several of which are depicted in a representative cell. External components include the glycocalyx, stretch-activated ion channels (SAC), cell-surface receptors, cell-cell or cell-matrix adhesion complexes. Internal components include the nucleus, cytoskeletal filaments, crosslinking proteins, and cell-signaling (autocrine/paracrine) molecules. Although the majority of mechanotransduction pathways to date have been investigated experimentally by applying tissue strains (compressive/tensile stresses) or fluid shear stresses across endothelial cell layers there is growing evidence that frictional shear stresses ($\tau = \mu P$) may also activate mechanobiological machinery in epithelial cell layers [27,33]. Adapted by permission from [24]Springer Nature: Mechanotransduction Gone Awry. Jaalouk DE and Lammerding J. Nat Rev Mol Cell Bio 2009; (10):63-73. License Number: 4780581421161

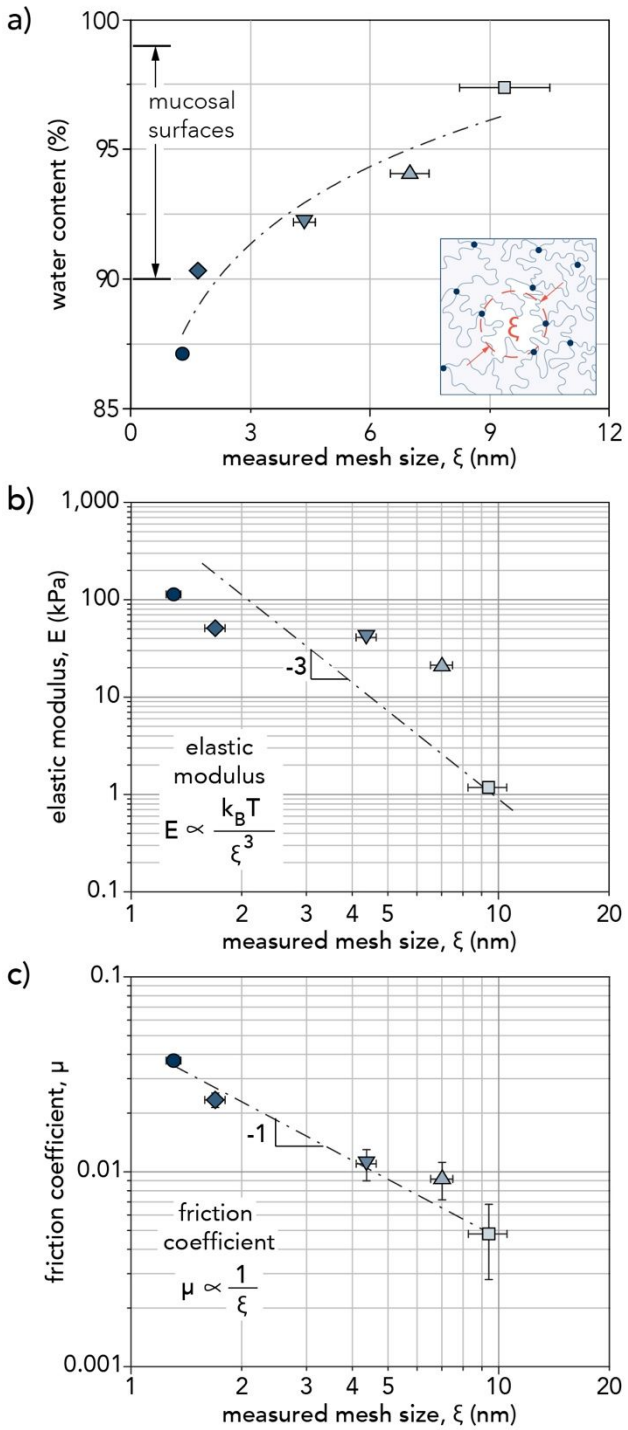

Fig. 3 The mechanical and transport properties of aqueous gels are controlled by a single parameter, the mesh size, ξ, which can be measured by small-angle X-ray scattering (SAXS). a) Increasing the characteristic mesh size of polyacrylamide hydrogels increases the water content. The inset illustrates the characteristic mesh size of a three-dimensional crosslinked hydrogel network [72]. Water content across various mucosal surfaces is typically 90-98% [65]. b) Increasing the mesh size dramatically decreases the elastic modulus with a -3 power-law scaling, as measured by microindentation using a solid hydrogel probe (radius of curvature, R = 2 mm) and a hydrogel disk (>4 mm thick, 30 mm radius) in a twinned or "Gemini"

configuration. The effective elastic modulus for each experiment was calculated from force-displacement curves of Gemini interfaces using Johnson-Kendall-Roberts (JKR) theory; maximum applied load, F_n = 2 mN, Poisson's ratio, v= 0.5. These results largely agree with de Gennes' predictions of elastic modulus scaling with mesh size to the inverse cubed power [64]. c) Increasing the mesh size decreases the friction coefficient with an inverse power-law scaling [72]. Adapted by permission from [72] Elsevier: Mesh Size Control of Polymer Fluctuation Lubrication in Gemini Hydrogels. Urueña JM, Pitenis AA, Nixon RM, Schulze KD, Angelini TE, Sawyer WG. Biotribology 2015; (1):24-29. License Number: 4780591083362

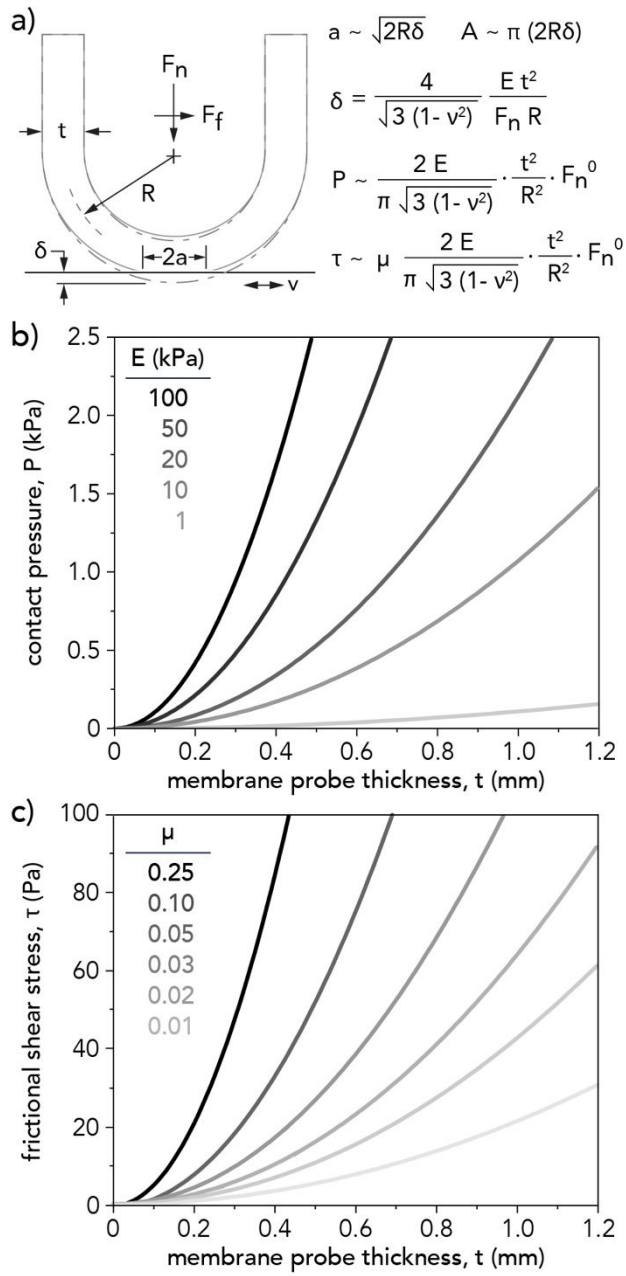

Fig. 4 Soft yet solid hydrogel probes (radius of curvature, R = 2 mm) impart exceedingly high Hertzian contact pressures to living cell layers, often leading to cell rupture. Instead, physiologically-relevant contact pressures may be achieved through hydrogel probes with spherical-cap membrane geometry. For a centrally-loaded spherical shell, the deflection, δ, is inversely related to the applied normal force, F_n; therefore, neither the contact pressure, P, nor frictional shear stress, τ, are functions of normal force [100,101]. Following Roark's analysis for a spherical shell membrane probe of radius of curvature R = 2 mm and Poisson's ratio of ν= 0.5 gives predictions for b) reducing contact pressures, either by reducing the membrane probe thickness, t, or by reducing the elastic modulus, E. and c) reducing frictional shear stresses, either by reducing the membrane probe thickness, t, or by reducing the friction coefficient, μ.

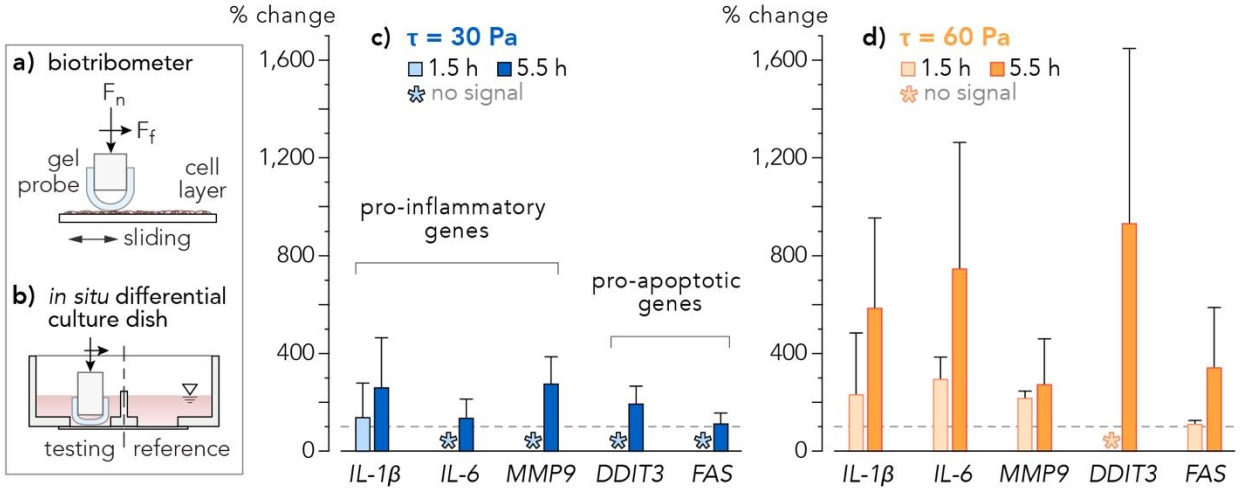

Fig. 5 a) Tribological tests were performed using a custom biotribometer, which applied normal forces to living cell layers with hydrogel membrane probes (E = 20 kPa, $t_{30\ Pa}$ = 0.8 mm and $t_{60\ Pa}$ = 1 mm), and measured friction forces during sliding in culture-like conditions (37 °C, 5% CO_2, and > 80% relative humidity). b) Roughly 200,000 human telomerase-immortalized corneal epithelial cells (hTCEpi) were plated on fibronectin-coated glass coverslips in each well of custom differential culture dishes and following tribological experimentation their gene expression profiles were compared to reference cell populations in adjacent yet isolated wells. c, d) Real time quantitative PCR analysis of RNA indicated that genes associated with the production of proinflammatory cytokines (*IL-1β, IL-6, MMP9*) and apoptosis (*DDIT3, FAS*) are upregulated within 900 sliding cycles (5.5 h). The degree of upregulation increased with increasing frictional shear stress (τ = 30 Pa to 60 Pa) and duration of sliding (1.5 h to 5.5 h), although the magnitude of frictional shear stress appears to be the predominant driver. Dashed line corresponds to noise threshold. Adapted by permission from [33]Springer Nature: Friction-Induced Inflammation. Pitenis AA *et al.* Trib Lett 2018; (66). License Number: 4780600009816

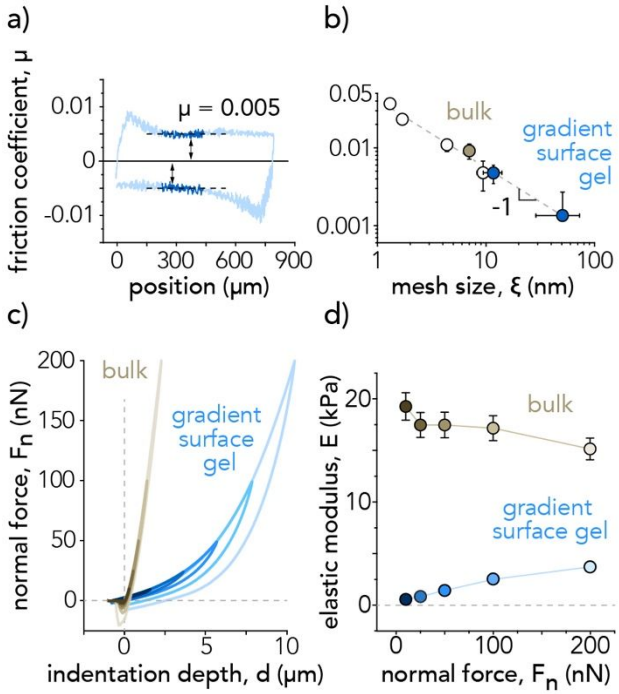

Fig. 6 a) Like many mucosal surfaces, synthetic gradient surface gels with a very high mesh size at the sliding surface may exhibit superlubricity, or ultra-low friction coefficients (μ < 0.01) in Gemini configurations [102]. b) "Gradient surface gels" (blue circles) exhibit much lower friction coefficients than aqueous gels polymerized with the same precursor solution but molded against flat polystyrene surfaces ("bulk", brown circle) [102]. c) Serial nanoindentations of increasing normal force (corresponding to lighter curves) show that the bulk (brown) exhibits uniformly Hertzian contact mechanics, whereas the gradient surface gel (blue) exhibits hysteretic and non-Hertzian contact mechanics. d) Nanoindentations suggest that gradient surface gels (blue circles) may be an order of magnitude softer than the bulk (brown circles).